

# LiZn<sub>2</sub>V<sub>3</sub>O<sub>8</sub>: A new geometrically frustrated cluster spin-glass

S. Kundu,<sup>1,\*</sup> T. Dey,<sup>2</sup> A. V. Mahajan,<sup>1</sup> and N. Büttgen<sup>3</sup>

<sup>1</sup>*Department of Physics, Indian Institute of Technology Bombay, Powai, Mumbai 400076, India*

<sup>2</sup>*Experimental Physics VI, Center for Electronic Correlations and Magnetism,  
University of Augsburg, 86159 Augsburg, Germany*

<sup>3</sup>*Experimental Physics V, Center for Electronic Correlations and Magnetism,  
University of Augsburg, 86159 Augsburg, Germany*

(Dated: January 1, 2020)

## Abstract

We have investigated the structural and magnetic properties of a new cubic spinel LiZn<sub>2</sub>V<sub>3</sub>O<sub>8</sub> (LZVO) through x-ray diffraction, dc and ac susceptibility, magnetic relaxation, aging, memory effect, heat capacity and <sup>7</sup>Li nuclear magnetic resonance (NMR) measurements. A Curie-Weiss fit of the dc susceptibility  $\chi_{dc}(T)$  yields a Curie-Weiss temperature  $\theta_{CW} = -185$  K. This suggests strong antiferromagnetic (AFM) interactions among the magnetic vanadium ions. The dc and ac susceptibility data indicate the spin-glass behavior below a freezing temperature  $T_f \simeq 3$  K. The frequency dependence of the  $T_f$  is characterized by the Vogel-Fulcher law and critical dynamic scaling behavior or power law. From both fitting, we obtained the value of the characteristic angular frequency  $\omega_0 \approx 3.56 \times 10^6$  Hz, the dynamic exponent  $z\nu \approx 2.65$ , and the critical time constant  $\tau_0 \approx 1.82 \times 10^{-6}$  s, which falls in the conventional range for typical cluster spin-glass (CSG) systems. The value of relative shift in freezing temperature  $\delta T_f \simeq 0.039$  supports a CSG ground states. We also found aging phenomena and memory effects in LZVO. The asymmetric response of the magnetic relaxation below  $T_f$  supports the hierarchical model. Heat capacity data show no long-range or short-range ordering down to 2 K. Only about 25% magnetic entropy change ( $\Delta S_m$ ) signifies the presence of strong frustration in the system. The <sup>7</sup>Li NMR spectra show a shift and broadening with decreasing temperature. The spin-lattice and spin-spin relaxation rates show anomalies due to spin freezing around 3 K as the bulk magnetization.

PACS numbers: 75.50.Lk, 75.40.Cx, 76.60.-k

## I. INTRODUCTION

Spinel oxides with the general formula AB<sub>2</sub>O<sub>4</sub> have provided an excellent arena for studying the effects of geometrical frustration [1, 2] and have seen a surge of interest in the past decade due to a series of exciting experimental observations. In the cubic spinel, the B-sites form a corner shared, 3D tetrahedral network like the pyrochlore lattice which is geometrically frustrated. Geometrical frustration arises when magnetic moments occupying the B-sites interact antiferromagnetically with each other. With the intention of unraveling novel magnetic properties arising due to geometric frustration, we were in the quest for new B-site cubic spinel compounds. In this category, 3d-transition metal oxide LiV<sub>2</sub>O<sub>4</sub> [3–5] (V<sup>3+</sup>: V<sup>4+</sup> = 1:1) is a well-studied system. It shows heavy fermion behavior [6]. But with non-magnetic impurity (Zn/Ti) doping, it shows spin-glass behavior [7–9]. Recently studied mixed valent spinel system Zn<sub>3</sub>V<sub>3</sub>O<sub>8</sub> or [Zn<sub>1.0</sub>(Zn<sub>0.25</sub>V<sub>0.75</sub>)<sub>2</sub>O<sub>4</sub>]<sub>2</sub> with V<sup>3+</sup>: V<sup>4+</sup> = 2:1 [10] has been suggested to possess a cluster spin-glass ground state. Similarly, Li<sub>2</sub>ZnV<sub>3</sub>O<sub>8</sub> (better written as [Zn<sub>0.5</sub>Li<sub>0.5</sub>(Li<sub>0.25</sub>V<sub>0.75</sub>)<sub>2</sub>O<sub>4</sub>]<sub>2</sub>) containing only V<sup>4+</sup> ( $S = 1/2$ ) magnetic ions shows spin-glass behavior at low temperatures [11]. LiZn<sub>2</sub>Mo<sub>3</sub>O<sub>8</sub> [12, 13] is another system stoichiometrically similar to our probed sys-

tem. With a frustrated geometry, it exhibits a resonating valence-bond condensed state [14]. The strong interplay between the spin, charge, lattice and orbital degrees of freedom in these transition metal oxides (TMO) are the source of these novel magnetic properties. Motivated by these exotic behaviors of the cubic spinels, we decided to investigate the mixed valent system LiZn<sub>2</sub>V<sub>3</sub>O<sub>8</sub> (LZVO). Only the structural and electrical properties of LZVO were reported long back in 1972 by B. Reuter and G. Colmann [15]. The magnetic properties of LZVO have not been reported so far. As zinc prefers the A-site in spinel like in ZnCr<sub>2</sub>O<sub>4</sub> [16, 17] and ZnV<sub>2</sub>O<sub>4</sub> [18, 19], we expect the site occupancy of LZVO to be represented as [Zn<sub>1.0</sub>(Li<sub>0.25</sub>V<sub>0.75</sub>)<sub>2</sub>O<sub>4</sub>]<sub>2</sub> - where the octahedral B-site is occupied by Li and V in the 1:3 ratio. It will be interesting to observe how the 25% dilution via non-magnetic lithium affects the magnetic properties of LZVO. Also, this system is amenable to nuclear magnetic resonance (NMR) local probe measurement of <sup>7</sup>Li nuclei. From stoichiometry, LZVO is a mixed valent spinel as in this compound the average vanadium valence is  $+\frac{11}{3}$ . So it will be interesting to see whether this leads to tetravalent and trivalent V in a 2:1 ratio.

The motivation behind studying the system LiZn<sub>2</sub>V<sub>3</sub>O<sub>8</sub> is to contrast its properties with those of the resonating valence bond solid and cluster magnet compound LiZn<sub>2</sub>Mo<sub>3</sub>O<sub>8</sub>, whereas Zn<sub>3</sub>V<sub>3</sub>O<sub>8</sub> (ZVO) was motivated by Majumdar-Ghosh chain system Ba<sub>3</sub>V<sub>3</sub>O<sub>8</sub>. Also, in LZVO, the effective spin value is close to  $S = 1/2$  whereas in ZVO the effective spin is close to

\*Electronic address: skundu37@gmail.com

$S = 1$ . As quantum fluctuations are more prominent in low spin systems, quantum effects in LZVO might play a dominant role compared to classical ZVO. Also,  $\text{Zn}_3\text{V}_3\text{O}_8$  (ZVO) has the ratio of  $\text{V}^{3+} : \text{V}^{4+} = 2:1$  whereas for LZVO it is 1:2. In contrast,  $\text{Li}_2\text{ZnV}_3\text{O}_8$  contains only  $S = 1/2 \text{ V}^{4+}$ . The strength of the exchange couplings reflected in the Curie-Weiss temperature  $\theta_{\text{CW}}$  is about -370 K for ZVO while for  $\text{Li}_2\text{ZnV}_3\text{O}_8$  it is about -210 K. For both ZVO and  $\text{Li}_2\text{ZnV}_3\text{O}_8$  the irreversible temperature is  $T_{\text{irr}} \simeq 6.0$  K and freezing temperatures ( $T_f$ ) is around 3.75 K and 3.50 K respectively.

In this work, we report sample preparation, structural analysis, bulk magnetic properties, heat capacity and  $^7\text{Li}$  NMR measurements on LZVO. The system crystallizes in the centrosymmetric  $Fd\bar{3}m$  space group with a site sharing between the lithium and the vanadium atoms at the crystallographic 16c sites. Our magnetization data show no long-range ordering down to 2 K but we found a splitting between the zero field cooled (ZFC) and field cooled (FC) data at 3 K in low fields. A large Curie-Weiss temperature,  $\theta_{\text{CW}} = -185$  K indicates strong antiferromagnetic (AFM) interactions between the magnetic ions. Our frequency dependent ac susceptibility results indicate a spin-glass ground state. To know the spin-dynamics of the glassy phase in detail, we have carried out further magnetization measurements below the freezing temperature ( $T_f$ ) and observed clear signature of magnetic relaxation, aging effect and memory phenomena which are thought to be typical characteristics of spin-glasses. In memory effects, we observed that a small heating cycle erases its previous memory and reinitializes the relaxation process. This type of asymmetric response favors by the hierarchical model [20, 21]. The inferred magnetic heat capacity has a broad maximum at  $T \sim 7$  K but no sharp anomaly indicative of long-range ordering (LRO) is observed. The field swept  $^7\text{Li}$  NMR spectra down to 1.8 K indicate the presence of an NMR line shift and gradual broadening of the spectra as  $T$  decreases. The spin-lattice and spin-spin relaxation rates both show anomalies at a freezing temperature of 3 K.

## II. EXPERIMENTAL DETAIL

The polycrystalline  $\text{LiZn}_2\text{V}_3\text{O}_8$  sample was prepared by conventional solid-state reaction techniques using high purity starting materials. The sample was prepared in two steps. First, we prepared the  $\text{LiZnVO}_4$  precursor from a stoichiometric mixture of preheated  $\text{Li}_2\text{CO}_3$  (99.995% pure),  $\text{ZnO}$  (99.9% pure) and  $\text{V}_2\text{O}_5$  (99.99% pure) at 700°C for 15 hours in a box furnace. After that,  $\text{LiZnVO}_4$ ,  $\text{V}_2\text{O}_3$  and  $\text{ZnO}$  were mixed well (in the molar ratio 1:1:1), pelletized and sealed in a quartz tube after flushing with argon gas. The sample was then fired in a box furnace for 24 hours with intermediate regrinding, pelletization and sealing. The temperatures during successive firing were 600°C and 700°C. Powder x-ray diffraction (XRD) measurements were performed at room

temperature (RT) with  $\text{Cu } K_\alpha$  radiation ( $\lambda = 1.54182 \text{ \AA}$ ) on a PANalytical X'Pert PRO diffractometer. Magnetization measurements were carried out in the temperature range 1.8 – 400 K and the field range 0 – 70 kOe using a Quantum Design SQUID VSM. For the low-field magnetization measurements, the reset magnet mode option of the SQUID VSM was used to set the field to zero. Heat capacity measurements were performed in the temperature range 1.8 – 295 K and in the field range 0 – 90 kOe using the heat capacity option of a Quantum Design PPMS. The NMR measurements were carried out using a phase-coherent pulse spectrometer on  $^7\text{Li}$  nuclei in a temperature range 1.8 - 200 K. We have measured field sweep  $^7\text{Li}$  NMR spectra, spin-spin relaxation rate ( $\frac{1}{T_2}$ ) and spin-lattice relaxation rate ( $\frac{1}{T_1}$ ) at two different fixed radio frequencies (rf) of about 95 MHz and 30 MHz, respectively. The spectra were measured using a conventional spin-echo sequence ( $\frac{\pi}{2} - \tau_{\text{echo}} - \pi$ ). We have used the spin-echo pulse sequence with a variable delay time  $\tau_D$  to measure  $T_2$  and a saturation pulse sequence ( $\frac{\pi}{2} - \tau_D - \pi$ ) is used after a waiting time or last delay of three to five times of  $T_1$  between each saturation pulse to measure  $T_1$ .

## III. RESULTS AND DISCUSSION

### A. Crystal structure

To check for phase purity, we have measured the XRD pattern of polycrystalline LZVO. The Rietveld refinement of LZVO (shown in Fig. 1) revealed that it crystallizes in the centrosymmetric cubic spinel  $Fd\bar{3}m$  (227) space group. The two phase refinement of LZVO indicates the presence of non-magnetic impurity phase  $\text{Li}_3\text{VO}_4$  (less than 2%) together with the main phase. The atomic positions obtained after Rietveld refinement (using Fullprof suite [22]) are given in Table I. After refinement, we obtained the lattice parameters as :  $a = b = c = 8.364 \text{ \AA}$ ,  $\alpha = \beta = \gamma = 90^\circ$ . The goodness of the Rietveld refinement is inferred from the following parameters  $\chi^2$ : 1.37;  $R_p$ : 21.8%;  $R_{\text{wp}}$ : 10.7%;  $R_{\text{exp}}$ : 9.14%.

Note that from Rietveld refinement we can rewrite the chemical formula of  $\text{LiZn}_2\text{V}_3\text{O}_8$  as  $[\text{Zn}_{1.0}(\text{Li}_{0.241}\text{V}_{0.759})_2\text{O}_4]_2$  like the cubic spinel general formula  $\text{AB}_2\text{O}_4$ . One unit cell is shown in Fig. 2(a). Here the  $\text{Zn}^{2+}$  ions are at the tetrahedral A-sites and connected to other  $\text{Zn}^{2+}$  ions like in a diamond structure and the octahedral B-sites are statistically occupied by  $\text{Li}^{1+}$  and vanadium ions (both  $\text{V}^{3+}$  and  $\text{V}^{4+}$ ) in a 1:3 ratio. The V-V bond distance is 2.95 Å. The vanadium occupies the octahedral B-site and among themselves they form a corner shared tetrahedral network like in the pyrochlore lattice which is geometrically frustrated. Random or statistical distribution between the  $\text{Li}^{1+}$ ,  $\text{V}^{3+}$  and  $\text{V}^{4+}$  ions dilutes the corner-shared tetrahedral magnetic network. This dilution works as an additional source of disorder and forces the system to relieve

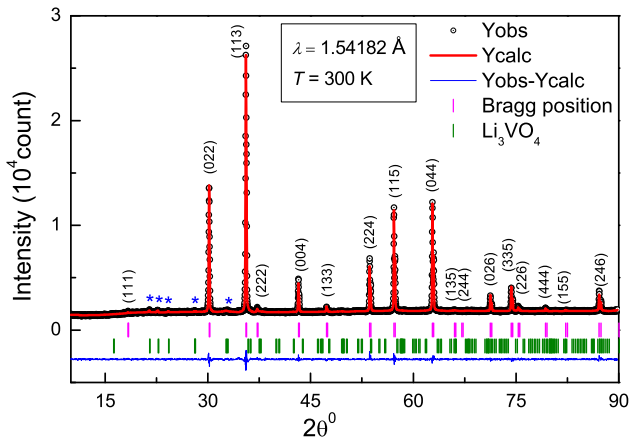


Figure 1: Powder XRD pattern of LZVO at 300 K and its Rietveld refinement considering  $Fd\bar{3}m$  space group is shown along with its Bragg peak positions (pink vertical bars) and the corresponding Miller indices (hkl). The black circles are the observed data, the red solid line is the calculated Rietveld pattern, the blue solid line is the residual data and the olive vertical bars are the Bragg peak positions for the non-magnetic impurity  $\text{Li}_3\text{VO}_4$ . The main peaks of  $\text{Li}_3\text{VO}_4$  are indicated by blue asterisks.

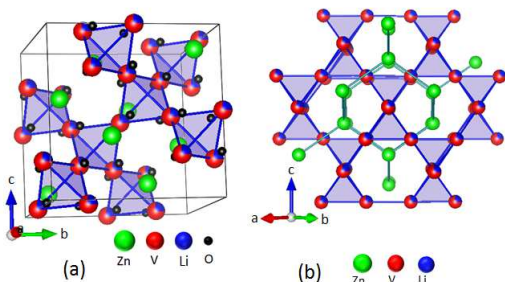


Figure 2: (a) One unit cell of LZVO. (b) Corner shared tetrahedral network of magnetic vanadium atoms and corner shared diamond structure of  $\text{Zn}^{2+}$  ions.

the frustration and a spin-glass or frozen state might emerge. Fig. 2(a) and (b) shows  $(\text{Li}/\text{V})_4$  corner shared tetrahedra in 3D.

Table I: Atomic positions in  $\text{LiZn}_2\text{V}_3\text{O}_8$  after Rietveld refinement of powder XRD at room temperature.

Atom	Wyckoff position	x/a	y/b	z/c	Occupancy
Zn	8b	0.375	0.375	0.375	1.000
Li	16c	0.000	0.000	0.000	0.241
V	16c	0.000	0.000	0.000	0.759
O	32e	0.239	0.0.239	0.239	1.000

## B. DC susceptibility

The magnetization ( $M$ ) of LZVO was measured as a

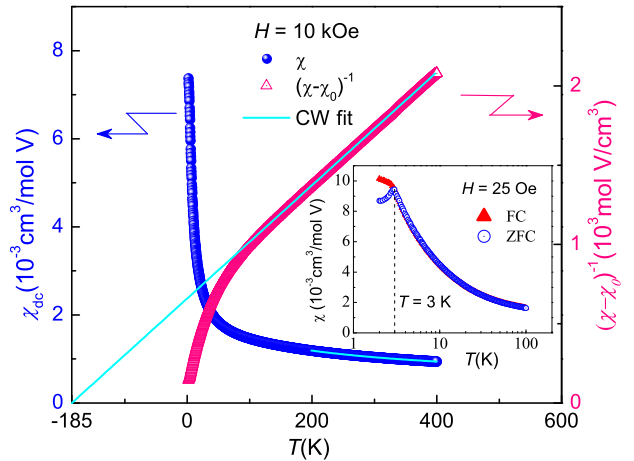


Figure 3: The dc susceptibility  $\chi_{dc}(T)$  (on left  $y$ -axis) and the inverse susceptibility free from  $T$ -independent  $\chi$  (on right  $y$ -axis) of LZVO in  $H = 10$  kOe are depicted as a function of temperature. The solid lines show the Curie-Weiss fit. In the inset, the bifurcation between zero field cooled (ZFC) and field cooled (FC) data below  $T_f = 3$  K is observed in an applied field of 25 Oe.

function of temperature ( $T$ ) at various applied magnetic fields ( $H$ ). The dc susceptibility ( $\chi_{dc}(T) = \frac{M}{H}$ ) is plotted as a function of temperature in an applied field  $H = 10$  kOe in Fig. 3. There is no long-range or short-range ordering down to 2 K. The  $\chi_{dc}(T)$  in  $H = 10$  kOe is paramagnetic and follows a Curie-Weiss law. The zero field cooled (ZFC) and field cooled (FC) data in  $H = 10$  kOe show no difference down to 2 K. From a Curie-Weiss fit of  $\chi_{dc}(T)$  using the equation:  $\chi(T) = \chi_0 + \frac{C}{(T - \theta_{CW})}$  in the range of (200 - 400) K, we obtained the temperature independent susceptibility  $\chi_0 = 4.62 \times 10^{-4}$  ( $\text{cm}^3/\text{mol V}$ ), the Curie constant  $C = 0.28 \text{ Kcm}^3/\text{mol V}$  and the Curie-Weiss (CW) temperature,  $\theta_{CW} = -185$  K. The effective moment  $\mu_{\text{eff}}$  is then about  $1.50 \mu_B$  which is less than that of the  $\mu_{\text{eff}} = 1.73 \mu_B$  for a spin  $S = \frac{1}{2}$  system. From the stoichiometry of LZVO, one might have expected two  $\text{V}^{4+}$  ions and one  $\text{V}^{3+}$  ion per formula unit giving a Curie constant  $C = 0.583 \text{ cm}^3\text{K}/\text{mol V}$ . However, we inferred a much smaller value. This result is similar to the homologous cluster magnet  $\text{LiZn}_2\text{Mo}_3\text{O}_8$  [12] where the Curie constant ( $C = 0.24 \text{ Kcm}^3/\text{mol f.u.}$ ) was less than the expected value. In metallic  $\text{LiV}_2\text{O}_4$ , the Curie constant was found to be that corresponding to one  $S = \frac{1}{2}$  moment per vanadium whereas one has, on an average, 1.5 electrons per vanadium. It is possible that here as well, the moment is quenched to some extent due to frustration. The high CW temperature suggests strong antiferromagnetic interactions between the magnetic vanadium atoms in the sample. In the inset of Fig. 3, the susceptibility, in a low field of 25 Oe, in ZFC (open circles) and FC (closed triangles) mode shows bifurcation below  $T_f \simeq 3$  K. This bifurcation suggests a spin-glass (SG) ground state of the system at low temperature. The inferred frustration parameter [1] ( $f = \frac{|\theta_{CW}|}{T_N} \approx 62$ ) puts

the LZVO system in the highly frustrated category.

### C. AC susceptibility

To further understand the nature of the SG states of LZVO, the ac magnetic susceptibility was measured in a fixed ac field of  $H_{ac} = 3.5$  Oe with  $T$ -range ( $2 \leq T \leq 4.2$  K) and frequency range  $1 \leq \nu \leq 1000$  Hz. The temperature variation of the in-phase component of the ac susceptibility,  $\chi'_{ac}(T)$ , as shown in Fig. 4, shows a cusp like behavior and a peak at  $T_f = 3.0$  K for  $\nu = 11$  Hz. The peak position shifts towards higher temperatures as the frequency  $\nu$  increases from 11 Hz to 555 Hz. So the frequency dependence of  $\chi'_{ac}(T)$  is evident with a downward shift of the anomaly with increasing  $\nu$  and is consistent with SG systems. Even the out of phase component of ac susceptibility  $\chi''_{ac}(T)$  shows a peak at  $T_f$  which barely shifts with frequency variation (shown in the inset of Fig. 4). The value of  $\chi''_{ac}(T)$  is non-zero positive below  $T_f$  and is negative above  $T_f$ . This indicates the SG state is associated with frustrated magnets. Such behavior is

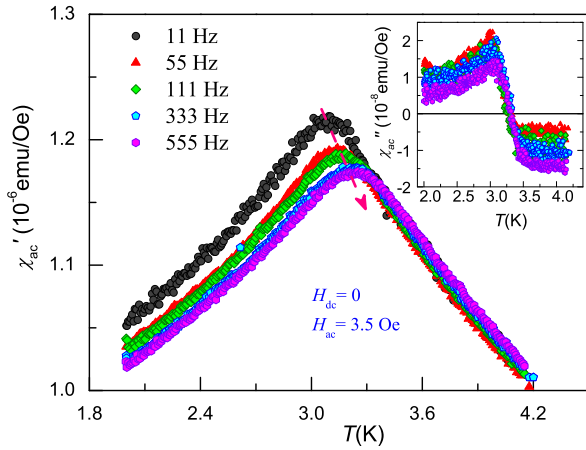


Figure 4: The temperature dependence of the in phase  $\chi'_{ac}$  (in main figure) and the out of phase  $\chi''_{ac}$  component (in the inset) of ac susceptibility ( $\chi_{ac}$ ) at different frequencies are shown.

distinctive of the SG states and allows us to categorize the SG systems from the disordered antiferromagnetic (AFM) systems. In the disordered AFM systems, the value of  $\chi''_{ac}(T)$  is constant and remains zero below the transition temperature [23–25]. All these features confirm the formation of a SG ground state of LZVO.

The frequency dependence of  $T_f$  is often quantified in terms of the relative shift of the spin freezing temperature, defined as  $\delta T_f = [\Delta T_f / T_f \Delta \log_{10}(\nu)]$  [26]. This relative shift parameter  $\delta T_f$  which is also known as Mydosh parameter [27] is used to identify different SG systems. The calculated value is  $\delta T_f \simeq 0.039$  for our LZVO. This value of  $\delta T_f$  indicates that the sensitivity to the frequency of LZVO is larger by an order of magnitude than that for canonical SG systems such as CuMn ( $\delta T_f = 0.005$ ) [28] and AuMn ( $\delta T_f = 0.0045$ ) [24]. Indeed,

it is intermediate between the values for canonical SG systems and superparamagnets ( $\delta T_f \simeq 0.28$ ). Also the present value of  $\delta T_f$  is close to that of the shape memory alloys showing re-entrant spin-glass (RSG) behavior [29], 0.037 seen in metallic glasses [30] and 0.095 reported in  $\text{LaCo}_{0.5}\text{Ni}_{0.5}\text{O}_3$  [31].

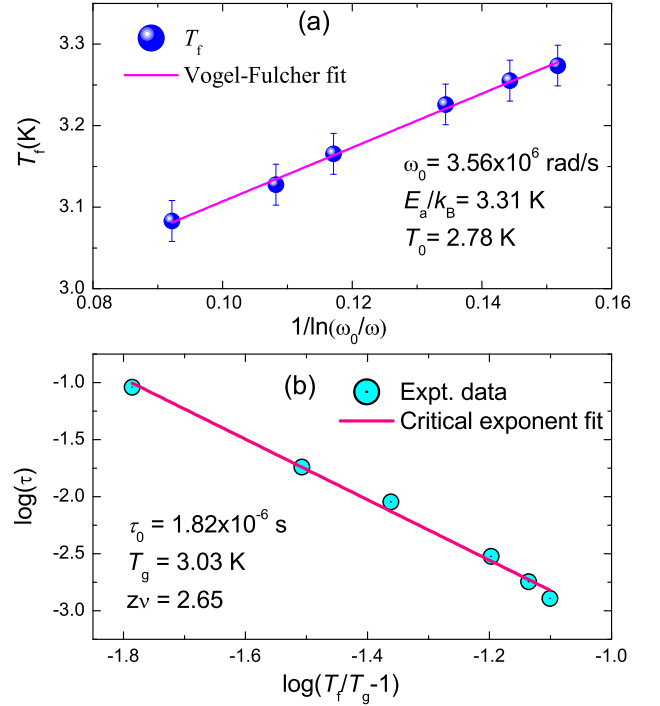


Figure 5: Frequency dependence of the freezing temperature  $T_f$  along with (a) the fit to the Vogel-Fulcher law. (b) the fit to the critical slowing down formula (see text).

To know the dynamic properties of the spins, we have fitted  $T_f$  with the empirical Vogel-Fulcher law:  $\omega = \omega_0 \exp[-\frac{E_a}{k_B(T_f - T_0)}]$  in Fig. 5(a). Here  $\omega_0$  is the characteristic angular frequency,  $\omega$  is the angular frequency ( $\omega = 2\pi\nu$ ),  $E_a$  and  $T_0$  are the activation energy and Vogel-Fulcher temperature, respectively. The best fit, shown in Fig. 5(a), is obtained for  $\omega_0 \approx 3.56 \times 10^6$  Hz,  $E_a/k_B \approx 3.31 \pm 0.10$  K, and  $T_0 \approx 2.78 \pm 0.01$  K. As the measured frequency range is limited (only up to 1 kHz), the error bar will be high in the derived parameters from such a fit. The Vogel-Fulcher fit of the variations of the freezing temperature ( $T_f$ ) with frequency suggests short-range Ising SG behavior [32]. The value of  $\omega_0$  obtained from the fitting is less than that of conventional SG systems, which is expected to be about  $10^{13}$  rad/s. Such a low value of  $\omega_0$  is associated with the re-entrant spin-glass (RSG) systems like  $\text{Ni}_2\text{Mn}_{1.36}\text{Sn}_{0.64}$  [29] and cluster spin-glass (CSG)  $\text{Zn}_3\text{V}_3\text{O}_8$  [10]. Thus we might suggest that the spin glass state in LZVO is not atomic in origin; rather it is related to flipping of large number of spins simultaneously or in a collective manner which leads to the formation of CSG states.

On further analysis, the  $T_f$  is found to obey the critical



slowing down dynamics (see Fig. 5(b)) governed by the equation:  $\tau = \tau_0 \left(\frac{T_f}{T_g} - 1\right)^{-zv}$ , where  $\tau_0$  is spin flipping relaxation time of the fluctuating entities,  $zv$  is the dynamic exponent and  $T_g$  is the static freezing temperature [33]. We found the best fit with  $T_g = 3.03 \pm 0.01$  K,  $\tau_0 \approx 1.82 \times 10^{-7}$  s and  $zv \approx 2.65$ . For the conventional SG systems, the value of  $\tau_0$  ranges within  $10^{-10}$  to  $10^{-13}$  s and  $zv$  in the range (4 - 13) [30]. The fact that the present value of  $\tau_0$ , is higher than that of the conventional SG systems, suggests that in LZVO, the spin-dynamics develops at a slower rate due to the presence of randomly magnetized interacting clusters, instead of individual spin randomness. Similar values have also been reported in SG systems such as Heusler alloys,  $\text{LaCo}_{0.5}\text{Ni}_{0.5}\text{O}_3$ , pyrochlore molybdates etc. [29, 31, 34]. The value of  $zv$  falls in the range of other typical CSG systems.

#### D. Aging effect and relaxation

Aging effect is a characteristic signature of any glassy system [28, 35]. Aging indicates that the response of a system becomes slower and slower with time. Here, aging effect has been studied with time evolution of zero field cooled (ZFC) magnetization. The Fig. 6(a) depicts the growth of the magnetization data as a function of time, in the frozen state. The sample was cooled from RT to 2.2 K in the ZFC mode and then the system was allowed to age for a waiting time  $t_w$ . Subsequently, a field of 200 Oe was applied and the magnetization was then recorded as a function of time. We have measured aging effect for three different waiting times 10 s, 1000 s and 5000 s. It is clear that the magnetization growth is slower for larger waiting times, which indicates the metastability of the low temperature magnetic state. We also measured the isothermal remanent magnetization ( $M_{\text{IRM}}$ ) of LZVO to explore the metastable behavior of the SG state around the SG transition temperature. To measure the  $M_{\text{IRM}}$ , first we cooled the sample in the ZFC mode from RT to the desired temperature mainly below the transition point, then we applied a field of 500 Oe and we switched off the field after 300 s and allowed the system to relax. During relaxation, we recorded the magnetization as a function of time for two hours. Fig. 6(b) shows seven relaxation curves which are normalized to the magnetization before making the field zero,  $M_{\text{IRM}}(t)/M_{\text{IRM}}(0)$  at seven different temperatures. The time dependence of  $M_{\text{IRM}}(t)$  is well fitted with the stretched exponential given as in equation  $M_t(H) = M_0(H) + [M_\infty(H) - M_0(H)][1 - \exp\{- (t/\tau)^\alpha\}]$ . Here,  $M_0$  and  $M_\infty$  are magnetizations at  $t \rightarrow 0$  and  $t \rightarrow \infty$ ,  $\tau$  is the characteristic relaxation time and  $\alpha$  is the stretching exponent, which ranges between 0 and 1. Depending on the value of  $\alpha$ , one can have an estimation of the distribution of energy barriers present in the frozen state. The obtained best fit parameters for each isotherm are listed in Table II. We have found that the values of  $\alpha$  for LZVO, varies within 0.45 to 0.55, is consistent with earlier reported glassy systems [10, 27, 36]. Also  $\alpha < 1$  indicates the anisotropic nature of energy barriers i.e.

the presence of metastable states in our LZVO system. From the value of  $\tau$ , it is evident that the decay is faster as the temperature near  $T_f \simeq 3$  K. This also signifies that LZVO system goes to a metastable and irreversible state below  $T_f$  on application of field. As expected, when  $T \geq T_f$ ,  $M_{\text{IRM}}(t)$  is independent of time.

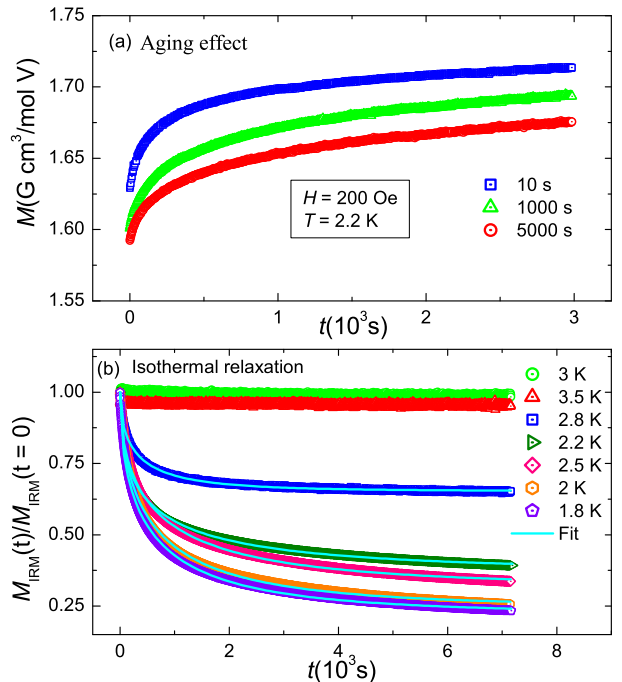


Figure 6: (a) Aging effect shows the growth of the magnetization as a function of time with three different waiting times and (b) Isothermal remanent magnetic relaxations (normalized with respect to the moment at  $t = 0$ ) with their fitting (described in text) are shown as a function of time at several temperatures.

Table II: The best fit (see text) result of isothermal remanent magnetic relaxation of LZVO.

$T$ (K)	$\frac{M_\infty}{M_0}$	Stretching exponent $\alpha$	Relaxation time $\tau$ (s)
1.8	0.223	0.53	580
2.0	0.248	0.55	649
2.2	0.372	0.46	593
2.5	0.318	0.52	737
2.8	0.653	0.54	323

#### E. Memory effect

Fig. 7 shows a memory effect which is measured in the FC magnetization mode using the protocol introduced by Sun *et al.* [20]. In an applied field of  $H = 500$  Oe, we have recorded the magnetization of LZVO as a function of temperature from 100 K down to 2 K with a cooling rate of 1 K/min. Below  $T_f$ , We interrupted the cooling

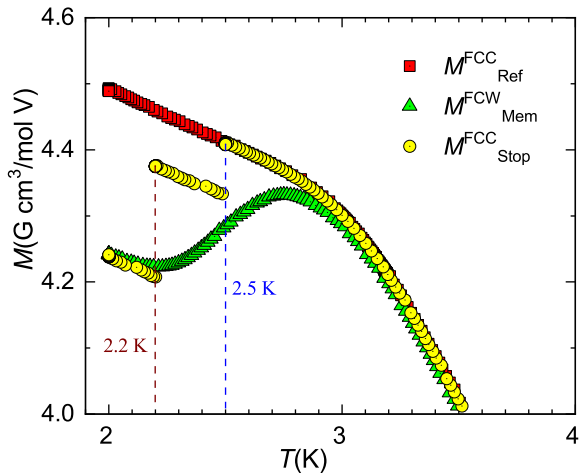


Figure 7: The memory effect in LZVO as a function of temperature is observed in FC magnetization mode at  $H = 500$  Oe. The  $M_{\text{Stop}}^{\text{FCC}}$  curve was obtained during cooling the sample with intermediate stops of 3 hours duration each at 2.5 K and 2.2 K. The  $M_{\text{Mem}}^{\text{FCW}}$  and  $M_{\text{Ref}}^{\text{FCC}}$  curves were measured during continuous heating and cooling of the sample respectively at  $H = 500$  Oe.

process twice at 2.5 K and 2.2 K for a waiting time  $t_w = 3$  hr each. We switched off the field during  $t_w$  and let the system to relax. We resumed the FC process after each stop and wait period. The stops at 2.5 K and 2.2 K are obvious as step-like features obtained in the  $M_{\text{Stop}}^{\text{FCC}}$  curve shown in Fig. 7. After reaching 2 K, we heated the sample continuously in the same magnetic field and recorded the magnetization data simultaneously. The magnetization obtained in this way, referred to as  $M_{\text{Mem}}^{\text{FCW}}$ , exhibits a slight inflexion at 2.5 K and a pronounced minimum at 2.2 K. This indicates that somehow the system has its previous behavior imprinted as a memory during the cooling process. Similar behavior has been noticed earlier in intermetallic compounds such as GdCu [36], Nd<sub>5</sub>Ge<sub>3</sub> [37] and in super-spin-glass nanoparticle systems [20, 38]. This is nothing but the typical aspect of SG systems. The inflexion point or dip at 2.5 K in the  $M_{\text{Mem}}^{\text{FCW}}$  curve is weak because at 2.5 K the system is not much below the freezing temperature (*i.e.*  $T_f = 3.0$  K at  $H = 500$  Oe). A reference curve ( $M_{\text{Ref}}^{\text{FCC}}$ ) was also measured by cooling the sample continuously at  $H = 500$  Oe. It is worth noting that there was no memory effect when we wait at a temperature above  $T_f$ .

*Negative heating cycle:* The memory effect was further clarified by the ZFC and FC method with a negative heating cycling as shown in Fig. 8. In the ZFC mode, we cooled the sample below the spin freezing temperature ( $T_f$ ) in zero field from the paramagnetic state to the measuring temperature  $T_1 = 2.75$  K. Then we recorded the magnetization as a function of time ( $t$ ) for 1 hr in an applied field of 500 Oe. The magnetization increases logarithmically with  $t$ . After that, we cooled the sample temperature to a lower value  $T_2 = 2.0$  K in the same field

and then we have measured the magnetization for a time  $t_2 = 1$  hr. Finally, we restored the sample temperature to  $T_1 = 2.75$  K and measured the magnetization for a period of  $t_3 = 1$  hr. The relaxation curve obtained in this way is shown in Fig. 8(a). In each relaxation process, the magnetization increases logarithmically with  $t$  and the system remembers its previous value it reached before the temporary cooling started. This determines that the negative  $T$ -cycle does not erase the memory in ZFC mode. For the FC mode, we field cooled the sample to  $T_1 = 2.75$  K first in a field of 500 Oe. Once we reached the measuring temperature, we switched off the field and subsequently measured the magnetization as a function of time. Fig. 8(b) shows the FC relaxation process where the magnetization decays exponentially with  $t$ . Similarly, the FC method also preserves the state of the system even after a temperature cooling. Inset of Fig. 8 (a) and (b) shows that in both ZFC and FC methods, the magnetic relaxation during  $t_3$  is a continuation of the relaxation curve during  $t_1$ . This is a simple demonstration of the memory effect.

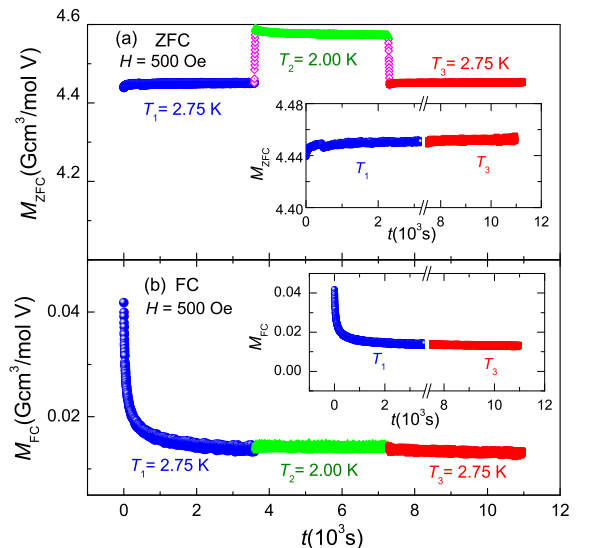


Figure 8: The magnetic relaxation in LZVO at 2.75 K with a negative heating cycle at  $H = 500$  Oe for (a) the ZFC and (b) the FC methods. The insets show the relaxation data during  $T_1$  and  $T_3$  which are merged in a seamless manner.

*Positive heating cycle:* The droplet model [39, 40] of SG systems supports a symmetric behavior in the magnetic relaxation concerning either heating or cooling cycles whereas the hierarchical model [20, 21] predicts an asymmetric response. To compare the response of intermittent heating and cooling cycles, we performed the relaxation experiment with a positive heating cycle also. The results are shown in Fig. 9(a) and (b). One might notice that a positive temperature cycle erases the earlier memory and re-initializes the relaxation process in both ZFC and FC mode. This confirms that the magnetic response of our system irrespective of heating or cooling cycle is not symmetric. So this study sup-

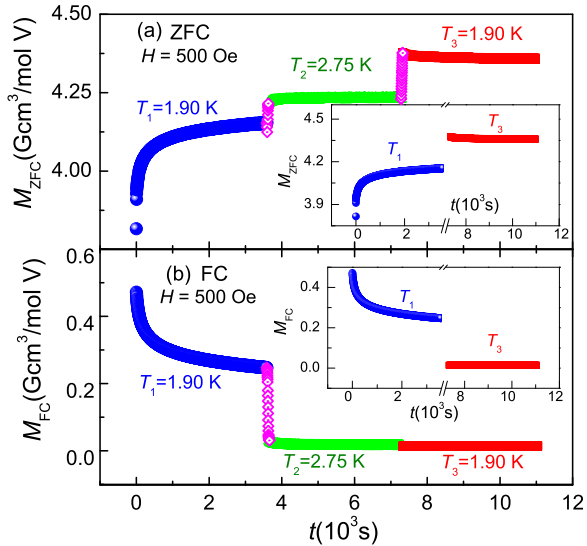


Figure 9: The magnetic relaxation in LZVO at 1.9 K with a positive heating cycle in  $H = 500$  Oe (a) the ZFC and (b) the FC methods. Insets show the relaxation data during  $T_1$  and  $T_3$  which are not merged.

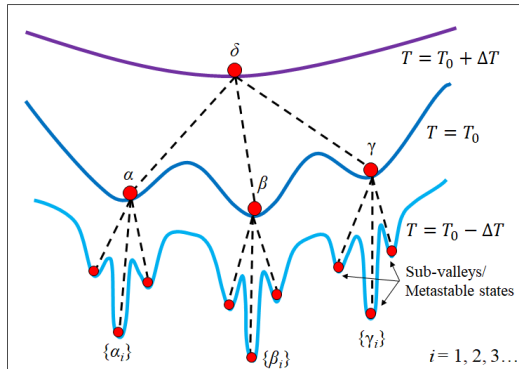


Figure 10: Schematic diagram of the hierarchical model for spin-glass states. The different curves represent the free energy at that particular temperatures. The metastable states of the spin-glass are depicted by the lobes at  $T = T_0 - \Delta T$ .

ports the hierarchical model proposed for SG systems. Fig. 10 depicts the schematic diagram of the hierarchical model. At a given temperature  $T_0$ , there exists a multi-valley  $\{\alpha, \beta, \gamma\}$  free-energy surface for a frustrated system. When we cool the system from  $T_0$  to  $T_0 - \Delta T$ , each valley splits into many sub-valleys  $\{\alpha_i\}, \{\beta_i\}, \{\gamma_i\}$ . When  $\Delta T$  is large, the energy gaps between the primary valleys become high and the system fails to overcome this energy barrier within a finite waiting time  $t_2$ . Therefore, the relaxation occurs only within the sub-valleys or metastable states. When the temperature of the system is restored to its initial value  $T_0$ , then the sub-valleys merge back to the original free energy surface and relaxation at  $T_0$  resumes without being perturbed by the intermediate relaxations at  $T_0 - \Delta T$ . But, if we increased

the system temperature from  $T_0$  to  $T_0 + \Delta T$ , then the barriers between the free energy primary valleys becomes low or sometimes they even get merged. Then, the relaxations can easily take place within different valleys. When the temperature is lowered back to  $T_0$ , the relative occupancy of each energy valley does not remain the same as before even though free energy surface goes back to the original state. Thus the state of the system varies after a temporary heating cycle and results without a memory effect. The behavior we found in our system, has been seen in some other SG systems too [10, 20, 36, 37, 41].

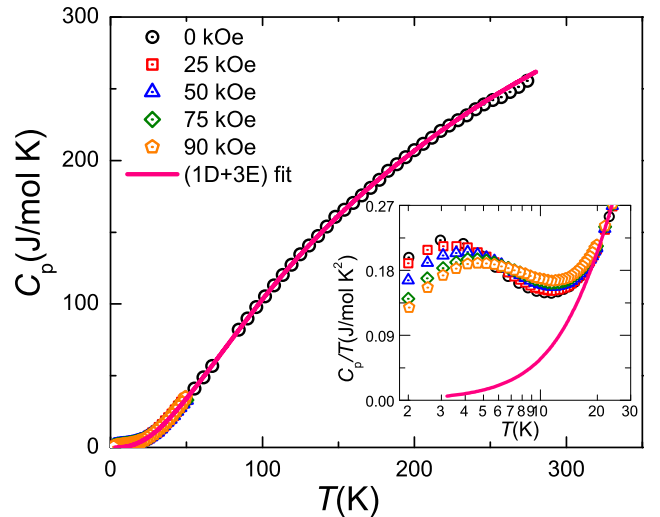


Figure 11: The heat capacity  $C_p(T)$  of LZVO as a function of temperature in different fields is plotted. The pink solid line represents the (Debye + Einstein) fit (see text) as well as the lattice heat capacity. The inset shows low temperature anomaly of  $C_p/T$  vs.  $T$  plot in semi-log scale.

## F. Heat capacity

We have measured the heat capacity of the LZVO sample at a constant pressure  $C_p(T)$  by the thermal relaxation method in different fields (0 - 90 kOe) at the temperature range (2 - 280) K for zero field and (2 - 50) K for higher fields. The Fig. 11 shows the temperature dependence of the specific heat at constant pressure  $C_p(T)$  of  $\text{LiZn}_2\text{V}_3\text{O}_8$ . Absence of sharp anomaly in the  $C_p(T)$  vs.  $T$  data implies a lack of long-range order in LZVO and supports our dc susceptibility data in  $H = 10$  kOe. Below 10 K, in the  $C_p/T$  vs.  $T$  plot (see inset of Fig. 11), there is a broad hump or anomaly at low temperature. These anomalies are field dependent and appear to be Schottky anomalies. To extract the magnetic contribution to the heat capacity, we have to subtract the lattice and Schottky contributions from the total heat capacity *i.e.* ( $C_m(T) = [C_p(T) - C_{\text{lat}} - C_{\text{Sch}}]$ ), where  $C_{\text{lat}}$  and  $C_{\text{Sch}}$  are the lattice and Schottky heat capacities respectively. As there is no suitable non-magnetic analog, we attempted to fit the specific heat capacity data with a combination of one Debye

term  $\left(C_d \left[9nR\left(\frac{T}{\theta_D}\right)^3 \int_0^{x_D} \frac{x^4 e^x}{(e^x - 1)^2} dx\right]\right)$  and several Einstein terms  $\left(\sum C_{e_i} \left[3nR\left(\frac{\theta_{E_i}}{T}\right)^2 \frac{\exp\left(\frac{\theta_{E_i}}{T}\right)}{\left(\exp\left(\frac{\theta_{E_i}}{T}\right) - 1\right)^2}\right]\right)$  to determine the  $C_{lat}$ . Among them, one Debye function plus three Einstein functions (1D+3E) fit was the best in the fit range 18 - 135 K. Here the coefficient  $C_d$  is the relative weight of the acoustic modes of vibration and coefficients  $C_{e1}$ ,  $C_{e2}$  and  $C_{e3}$  are the relative weights of the optical modes of vibrations. After fitting we obtained  $C_d:C_{e1}:C_{e2}:C_{e3} = 1:6:4:3$ . The sum of these coefficients is equal to the total number of atoms ( $n = 14$ ) per formula unit of LZVO. In the absence of an applied field,

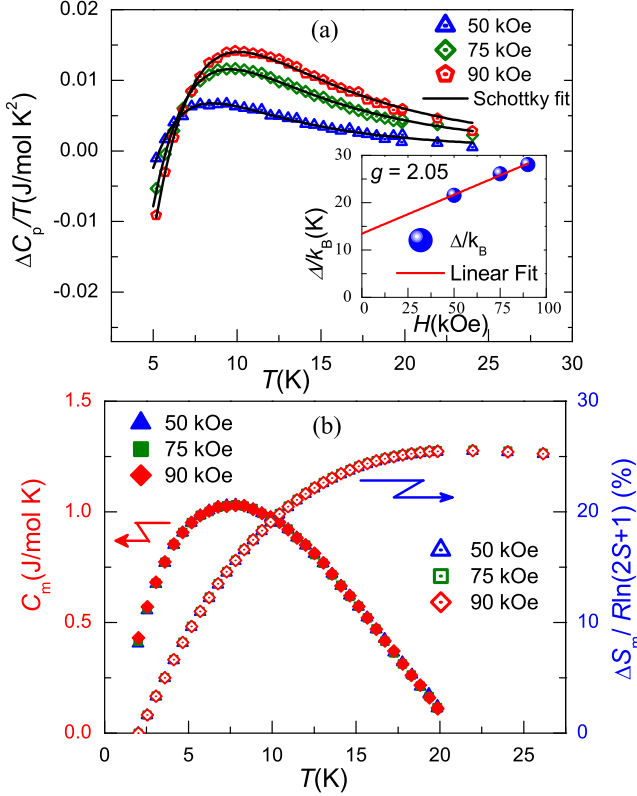


Figure 12: (a) It shows the low temperature Schottky anomaly fitting in different fields. The inset shows the linear dependence of the Schottky gap ( $\Delta$ ) with the field strength ( $H$ ). (b) The magnetic heat capacity ( $C_m$ ) on left  $y$ -axis and the magnetic entropy change ( $\Delta S_m$ ) on right  $y$ -axis of LZVO as a function of temperature is shown.

the  $C_p(T)$  data at  $H = 0$  kOe,  $C_p(0, T)$  contains lattice  $C_{lat}(T)$ , as well as a magnetic  $C_m(H, T)$  part but lacks a Schottky contribution. So we consider  $C_p(0, T)$  as a reference and subtract it from the higher field data  $C_p(H, T)$  to obtain Schottky contribution in that particular field,  $C_{Sch}(H, T) = [C_p(H, T) - C_p(0, T)] = \Delta C_p$ . Now this  $\Delta C_p$  represents the Schottky contribution provided that  $C_m(H, T)$  is field independent in that temperature range. In Fig. 12(a), we have plotted  $\Delta C_p/T$  vs.  $T$  and the Schottky contributions ( $C_{Sch}$ ) to the total heat capacity are well fitted by a two level Schottky sys-

tem  $C_{Sch} = f \left[ R \left( \frac{\Delta}{k_B T} \right)^2 \left( \frac{g_0}{g_1} \right) \frac{\exp\left(\frac{\Delta}{k_B T}\right)}{\left[ 1 + \left( \frac{g_0}{g_1} \right) \exp\left(\frac{\Delta}{k_B T}\right) \right]^2} \right]$  [42, 43]; where  $f$  is the fraction of free spins within the system,  $\Delta$  is the Schottky gap,  $R$  is the universal gas constant,  $k_B$  is the Boltzmann constant and  $g_0$  and  $g_1$  are the degeneracies of the ground state and excited state, respectively (in this case,  $g = g_0 = 1$ ). Here, with respect to the 25 kOe data, we have derived the Schottky contribution at higher fields as the zero field data have the same kind of anomaly present which might be a result of some intrinsic interactions present within the system. From the fitting of  $\Delta C_p(T)/T$ , we obtained the energy gap  $\Delta$  at different fields which are plotted in the inset of Fig. 12(a) and show a linear dependence. From the slope of  $\Delta/k_B$  vs.  $H$  plot, we obtained the value of Landé  $g$  factor,  $g = 2.05$  which is close to the value for free spin. From our fits, the fraction of  $S = \frac{1}{2}$  entities contributing to the heat capacity is about 2-5 %. The large intercept in the  $\Delta/k_B$  vs.  $H$  shows that the internal magnetism exists even in zero applied field as might be expected in a spin-glass. After subtracting the lattice and Schottky contribution, we obtained the magnetic heat capacity  $C_m$  at 50 kOe, 75 kOe and 90 kOe. Fig. 12(b) shows the magnetic heat capacity ( $C_m$ ) on the left  $y$ -axis. The  $C_m$  is independent of the applied field and it shows a hump around 7.5 K. Fig. 12(b) also shows the derived magnetic entropy change ( $\Delta S_m(T)$ ) on the right  $y$ -axis. The maximum value of  $\Delta S_m(T)$  ( $= \int \frac{C_m}{T} dT$ ) is 1.75 (J/mol K) which is only 25% of the expected  $R \ln(2S + 1) = 6.89$  (J/mol K) for two  $S = \frac{1}{2}$  spin ( $V^{4+}$  ions) and one  $S = 1$  spin ( $V^{3+}$  ion) per formula unit of LZVO. A large reduction of entropy change indicates quenching of moments due to frustration and/or the presence of many degenerate low-energy states at low temperature.

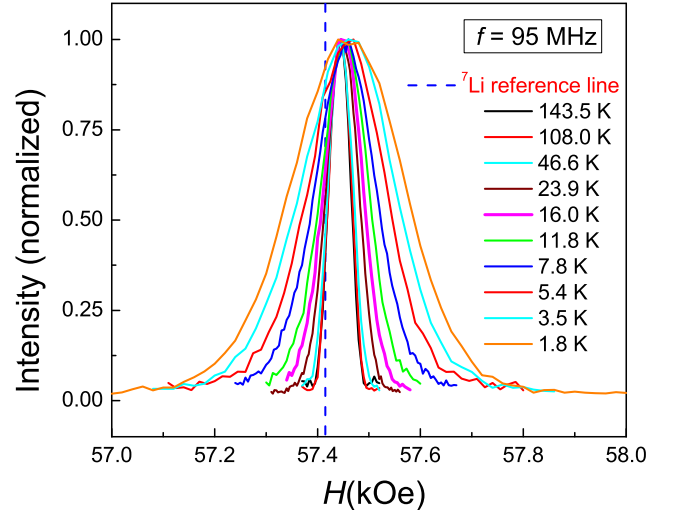


Figure 13: The  ${}^7\text{Li}$  NMR spectra of LZVO at different temperatures measured at a fixed frequency of 95 MHz. The blue dashed vertical line represents the reference position for  ${}^7\text{Li}$  nuclei at RT.



## G. ${}^7\text{Li}$ NMR spectra and shift

In LZVO, the non-magnetic Li ions and magnetic vanadium ions share the B-site. Due to a strong onsite coupling between the nuclear moment and the electronic moment it is difficult to detect NMR signal from the magnetic vanadium ions yielding very short relaxation times. For  $\text{Li}^{1+}$  ions, the electronic spin is zero ( $S = 0$ ), with a nuclear spin  $I = \frac{3}{2}$ . Additionally, the  ${}^7\text{Li}$  nuclei exhibit a high natural abundance (92.6%) and a high gyromagnetic ratio  $\frac{\gamma}{2\pi} = 1.6546$  MHz/kOe resulting in strong nuclear magnetization detectable in NMR experiments.  ${}^7\text{Li}$  NMR spectra have been measured at 95 MHz down to 1.8 K. The spin-lattice and spin-spin relaxation rates also have been measured to probe the low energy excitations.

Fig. 13 shows the spectra at different temperatures from 143 K to 1.8 K. The spectra get broadened and nominally shift towards higher fields (*i.e.* negative shift concerning frequency) as temperature decreases. By fitting the spectra at different temperatures to Gaussian functions we derived the full width at half maximum (FWHM) and NMR line shift  ${}^7K$  (using the relation  ${}^7K = \frac{H_{ref} - H_{res}}{H_{ref}}$ ; where  $H_{res}$  denotes the resonance field which is estimated by considering the peak position of that spectrum, while  $H_{ref}$  represents the reference field of the  ${}^7\text{Li}$  nuclei at room temperature). The calculated shift ( ${}^7K$ ) varies from -450 ppm (200 K) to -750 ppm (1.8 K) with respect to the  ${}^7\text{Li}$  NMR reference field  $H_{ref} = 57.415$  kOe at 95 MHz. The temperature dependence of FWHM and  ${}^7K$  are shown in Fig. 14 on the right and left  $y$ -axis, respectively. Both exhibit paramagnetic behavior according to the Curie-Weiss law of the bulk susceptibility  $\chi(T)$ . In the inset of Fig. 14, we have plotted the  ${}^7K(\%)$  vs. dc susceptibility  $\chi(T)$  with temperature as an implicit parameter and the linear behavior is seen. As  $K_{shift} = \frac{A_{hf}}{N_A \mu_B} \chi(T)$ ; the slope of the linear fit gives the hyperfine coupling constant ( $A_{hf}$ ). We have fitted the  ${}^7K$ - $\chi$  plot by a linear equation in two different ranges which are designated as linear fit 1 and linear fit 2. In linear fit 1, we have considered the whole temperature range and it gives us  $A_{hf} = (95 \pm 5)$  Oe/ $\mu_B$ . On the other hand, in linear fit 2, we have neglected a few low-temperature points (as, here, there could be some extrinsic Curie contribution due to paramagnetic impurities in the bulk susceptibility data) and this fit yields  $A_{hf} = (119 \pm 5)$  Oe/ $\mu_B$ .

## H. Spin-lattice and spin-spin relaxation

The spin-lattice relaxation time ( $T_1$ ) of  ${}^7\text{Li}$  at various temperatures was measured using a saturation recovery sequence at two fixed frequencies 95 MHz and 30 MHz. The data are well fitted with a single exponential ( $1 - \frac{M(t)}{M(0)} = Ae^{\frac{-t}{T_1}}$ ) in the temperature range (150 - 7 K). Around 3 K the data are best fitted with a stretched exponential. At low fields, the spin-lattice relaxation rate shows a prominent peak around 2.9 K which is close to the spin-glass ordering temperature  $T_f$

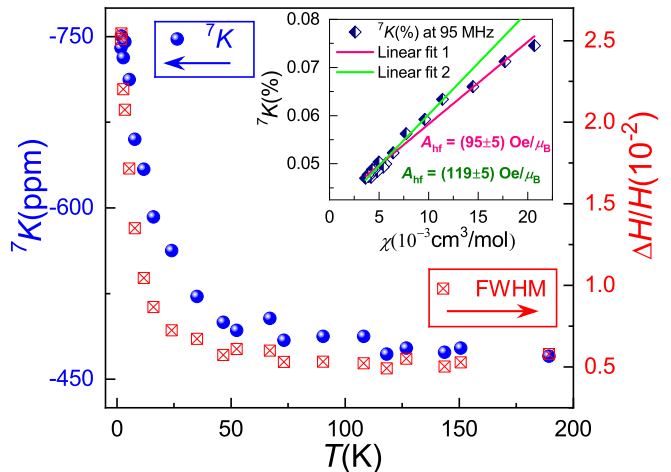


Figure 14: The  ${}^7\text{Li}$  NMR shift (left  $y$ -axis) and the FWHM (right  $y$ -axis) of the  ${}^7\text{Li}$  NMR spectra as a function of temperature behave like the paramagnetic bulk susceptibility. In the inset, the linear variation of  ${}^7K(\%)$  vs.  $\chi$  with temperature as an implicit parameter is shown and from the slope we determine the hyperfine coupling constant  $A_{hf}$ .

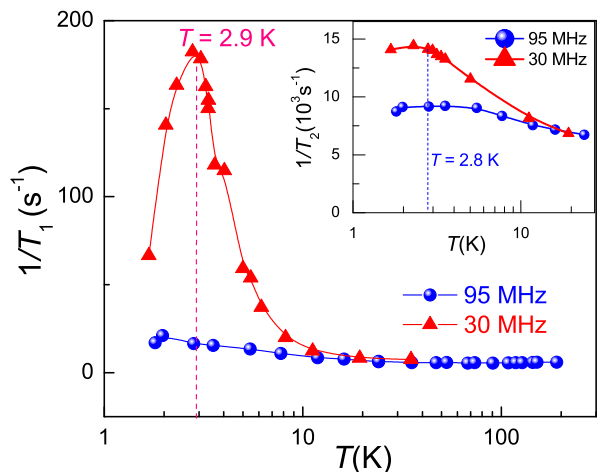


Figure 15: The spin-lattice relaxation rate ( $\frac{1}{T_1}$ ) and (in the inset) the spin-spin relaxation rate ( $\frac{1}{T_2}$ ) of  ${}^7\text{Li}$  are shown in semi-log scale. Both were measured at two different frequencies (95 MHz and 30 MHz) with a prominent peak at around  $T_f \simeq 3$  K in lower frequency according to a lower applied magnetic field. The connecting lines are a guides to the eye.

= 3 K (see Fig. 15). This is in agreement with the bulk dc susceptibility, where, in high fields, the anomaly is suppressed. The spin-spin relaxation data are well fitted with the single exponential ( $M(t) = M_0 e^{\frac{-2t}{T_2}}$ ). The spin-spin relaxation rates ( $\frac{1}{T_2}$ ) (see inset of Fig. 15) also show an anomaly around the SG transition temperature  $T_f \simeq 3$  K. The  ${}^7\text{Li}$  NMR  $\frac{1}{T_1}$  data at high-field is nearly unchanged with temperature, which is different from the published data of undoped  $\text{LiV}_2\text{O}_4$  [4] and doped  $\text{LiV}_2\text{O}_4$  [44] (see Fig. 16 where published data are shown along

with our data). In low-field *i.e.* at 30 MHz, we observed an increase in our  $\frac{1}{T_1}$  data of  $^7\text{Li}$  nuclei for LZVO near the freezing temperature  $T_f = 3$  K (see Fig. 15). Likewise in case of  $\text{Li}_{1-x}\text{Zn}_x\text{V}_2\text{O}_4$  ( $x = 0.1$ ) and  $\text{Li}(\text{V}_{1-y}\text{Ti}_y)_2\text{O}_4$  ( $y = 0.1$ ) [45], an anomaly or peak in the  $T$ -dependence of  $^7\text{Li}$  NMR  $\frac{1}{T_1}$  was seen close to the SG transition temperature. Also,  $^7\text{Li}$  NMR studies of  $S = \frac{1}{2}$  geometrically frustrated systems,  $\text{Li}_2\text{ZnV}_3\text{O}_8$  [11] and  $\text{LiZn}_2\text{Mo}_3\text{O}_8$  [13] have been reported with an almost temperature invariant spin-lattice relaxation rate ( $\frac{1}{T_1}$ ) of the order of  $10 \text{ s}^{-1}$  similar to what we have seen for our LZVO at 95 MHz. As the earlier reported spin-lattice relaxation data on pure and doped  $\text{LiV}_2\text{O}_4$  systems are measured at different frequencies, we have mentioned them in bracket for clarity in Fig. 16.

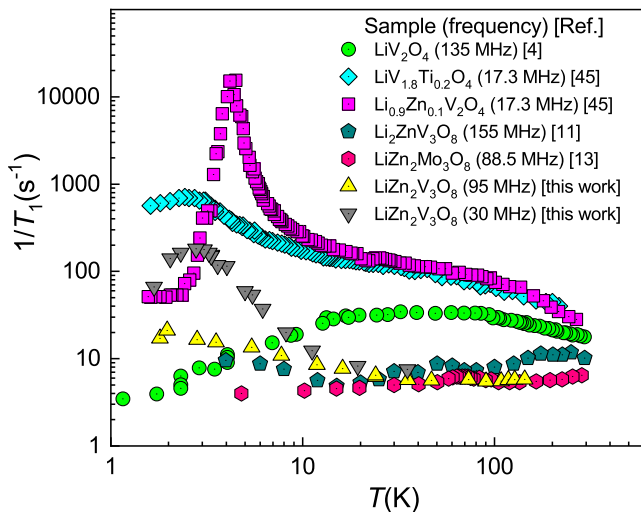


Figure 16: The spin-lattice relaxation rate ( $1/T_1$ ) of  $^7\text{Li}$  nuclei in LZVO is compared to the pure and doped  $\text{LiV}_2\text{O}_4$  systems from literature.

#### IV. DISCUSSION

Theoretical studies by M. Schmidt *et al.* [46], Gang Chen *et al.* [47–49] and E. C. Andrade *et al.* [50] show that when a geometrically frustrated system (like the Kagomé lattice) is driven by disorder then it often manifests spin-glass (SG) and sometimes cluster-spin-glass (CSG) properties. A sketch of the outcome is given in Fig. 17 which depicts a cartoon of spin orientation in a conventional SG and a CSG. The individual spins are locked in place for conventional SG systems whereas in CSG, a group of spins are locked to form a pair, triplet or even domains. The remaining spins which are not participating in the cluster are independent, but help to mediate the interactions between the clusters such that the clusters can change their sizes and response time. The bigger the cluster size, the slower is the relaxation rate. The clusters can be short-range ferromagnetic in

nature. But these need not to be fully FM entities; they can be mostly random with some correlation length which rigidly couples more than two spins.

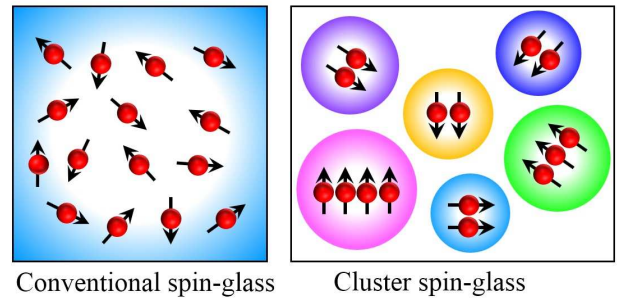


Figure 17: Illustration of conventional spin-glass and cluster spin-glass. The colors indicate the different domains formed by group of spins which are oriented in a particular direction with different magnetic strength.

Among the spinels where the pyrochlore lattice of the magnetic B-sites is diluted by non-magnetic ions in the ratio 1:3, for  $\text{LiZn}_2\text{V}_3\text{O}_8$  the Curie-Weiss temperature ( $\theta_{\text{CW}} = -185$  K) is somewhat lower than in  $\text{Li}_2\text{ZnV}_3\text{O}_8$  ( $\theta_{\text{CW}} = -214$  K) and much lower compared to  $\text{Zn}_3\text{V}_3\text{O}_8$  ( $\theta_{\text{CW}} = -370$  K). In all cases, the disorder at B-site of the spinel and the dilution of the corner-shared tetrahedral network in 3D due to the presence of 25% non-magnetic ions ( $\text{Zn}^{2+}$  for  $\text{Zn}_3\text{V}_3\text{O}_8$ ,  $\text{Li}^{1+}$  for  $\text{Li}_2\text{ZnV}_3\text{O}_8$  and  $\text{LiZn}_2\text{V}_3\text{O}_8$ ) triggers the system to form a spin-frozen state (cluster spin-glass rather than a conventional one) at about the same temperature. Considering the ratio of  $\text{V}^{3+}$  and  $\text{V}^{4+}$  ions, the expected Curie constant per vanadium is  $C = 0.79 \text{ Kcm}^3/\text{mol}$  for ZVO and  $C = 0.58 \text{ Kcm}^3/\text{mol}$  for LZVO; whereas the obtained values are  $C = 0.75 \text{ Kcm}^3/\text{mol}$  and  $C = 0.28 \text{ Kcm}^3/\text{mol}$ , respectively. We speculate that the much lower Curie constant in LZVO might indicate the presence of some degree of itinerancy like in the metallic  $\text{LiV}_2\text{O}_4$  system. It would be interesting to see how these parameters evolve with the extent of dilution.

#### V. CONCLUSION

The cubic spinel  $\text{LiZn}_2\text{V}_3\text{O}_8$  has been successfully synthesized. It crystallizes in the centrosymmetric cubic spinel  $Fd\bar{3}m$  space group. From a CW-fit of our 10 kOe dc susceptibility data, we obtained the Curie constant  $C = 0.28 \text{ Kcm}^3/\text{mol V}$  and CW temperature  $\theta_{\text{CW}} = -185$  K. The Curie constant suggests a possible suppression or partial quenching of local moments and the CW temperature suggests strong AFM interactions among the magnetic vanadium ions. A high value of frustration parameter ( $f \simeq 60$ ) is inferred from our data. The ZFC-FC bifurcation below  $T_f \simeq 3$  K indicates SG nature which is confirmed by frequency dependence of the ac susceptibility, the Vogel-Fulcher law and critical power law of the

$T_f$ . The low value of the characteristic angular frequency  $\omega_0 \approx 3.56 \times 10^6$  Hz and the high value of the critical time constant  $\tau_0 \approx 1.82 \times 10^{-6}$  s, corroborates the CSG ground state. The magnetic relaxation, aging phenomena and memory effect support the metastability of the CSG ground state. The asymmetric response in a positive temperature cycle obeys the hierarchical model proposed for the SG systems. Absence of any sharp anomaly in heat capacity data indicates lack of long-range ordering down to 2 K. The significant contribution of magnetic heat capacity shows a hump around 7.5 K which is independent of the applied field strength. The small entropy change ( $\Delta S_m \simeq 25\%$ ) presumably arises from a large degeneracy of the ground states. The field swept  ${}^7\text{Li}$  NMR spectra show a line shift ( ${}^7K$ ) as  $T$  decreases. The plot of line shift  ${}^7K$  (%) vs. bulk susceptibility  $\chi$  follows a linear behavior and the derived hyperfine coupling constant amounts to  $A_{\text{hf}} = 119$  Oe/ $\mu_B$ . The temperature depen-

dence of the spin-lattice relaxation rate ( $\frac{1}{T_1}$ ), and the spin-spin relaxation rate ( $\frac{1}{T_2}$ ) of the  ${}^7\text{Li}$  nuclei indicates that they are sensitive to the fluctuations of the magnetic ions and show an anomaly near  $T_f$ . All experimental results and observations point towards the formation of a CSG ground state in LZVO.

## VI. ACKNOWLEDGMENTS

SK acknowledges the central facility and financial support from IRCC, IIT Bombay. AVM would like to thank the Alexander von Humboldt foundation for financial support during his stay at Augsburg Germany. We kindly acknowledge support from the Deutsche Forschungsgemeinschaft (DFG, German Research Foundation) – Projekt Nummer 107745057 – TRR 80.

- 
- [1] J. E. Greedan, *J. Mater. Chem.* **11**, 37 (2001).
  - [2] R. Moessner and A. P. Ramirez, *Physics Today* **59**, 24 (2006).
  - [3] O. Chmaissem, J. D. Jorgensen, S. Kondo, and D. C. Johnston, *Phys. Rev. Lett.* **79**, 4866 (1997).
  - [4] S. Kondo, D. C. Johnston, C. A. Swenson, F. Borsa, A. V. Mahajan, L. L. Miller, T. Gu, A. I. Goldman, M. B. Maple, D. A. Gajewski, E. J. Freeman, N. R. Dilley, R. P. Dickey, J. Merrin, K. Kojima, G. M. Luke, Y. J. Uemura, O. Chmaissem, and J. D. Jorgensen, *Phys. Rev. Lett.* **78**, 3729 (1997).
  - [5] A. Krimmel, A. Loidl, M. Klemm, S. Horn, D. V. Sheptyakov, and P. Fischer, *Physica B: Condensed Matter* **350**, E297 (2004), proceedings of the Third European Conference on Neutron Scattering.
  - [6] G. R. Stewart, *Rev. Mod. Phys.* **56**, 755 (1984).
  - [7] W. Trinkl, A. Loidl, M. Klemm, and S. Horn, *Phys. Rev. B* **62**, 8915 (2000).
  - [8] K. Miyoshi, M. Ihara, K. Fujiwara, and J. Takeuchi, *Phys. Rev. B* **65**, 092414 (2002).
  - [9] Y. Ueda, N. Fujiwara, and H. Yasuoka, *Journal of the Physical Society of Japan* **66**, 778 (1997).
  - [10] T. Chakrabarty, A. V. Mahajan, and S. Kundu, *Journal of Physics: Condensed Matter* **26**, 405601 (2014).
  - [11] T. Chakrabarty, A. V. Mahajan, and B. Koteswararao, *Journal of Physics: Condensed Matter* **26**, 265601 (2014).
  - [12] J. P. Sheckelton, J. R. Neilson, D. G. Soltan, and T. M. McQueen, *Nature Materials* **11**, 493 (2012).
  - [13] J. P. Sheckelton, F. R. Foronda, L. Pan, C. Moir, R. D. McDonald, T. Lancaster, P. J. Baker, N. P. Armitage, T. Imai, S. J. Blundell, and T. M. McQueen, *Phys. Rev. B* **89**, 064407 (2014).
  - [14] P. Anderson, *Materials Research Bulletin* **8**, 153 (1973).
  - [15] B. Reuter and G. Colsmann, *Z. anorg. allg. Chem.* **894**, 138 (1972).
  - [16] S.-H. Lee, C. Broholm, T. H. Kim, W. Ratcliff, and S.-W. Cheong, *Phys. Rev. Lett.* **84**, 3718 (2000).
  - [17] S. Lee, C. Broholm, W. Ratcliff, G. Gasparovic, Q. Huang, T. H. Kim, and S. W. Cheong, *Nature* **418**, 856 (2002).
  - [18] S.-H. Lee, D. Louca, H. Ueda, S. Park, T. J. Sato, M. Isobe, Y. Ueda, S. Rosenkranz, P. Zschack, J. Íñiguez, Y. Qiu, and R. Osborn, *Phys. Rev. Lett.* **93**, 156407 (2004).
  - [19] M. Reehuis, A. Krimmel, N. Büttgen, N. A. Loidl, and A. Prokofiev, *Eur. Phys. J. B* **35**, 311 (2003).
  - [20] Y. Sun, M. B. Salamon, K. Garnier, and R. S. Averback, *Phys. Rev. Lett.* **91**, 167206 (2003).
  - [21] F. Lefloch, J. Hammann, M. Ocio, and E. Vincent, *Europhys. Lett.* **18**, 647 (1992).
  - [22] J. Rodriguez-Carvajal, *Physica B: Condensed Matter* **192**, 55 (1993).
  - [23] A. Malinowski, V. L. Bezusyy, R. Minikayev, P. Dziawa, Y. Syryanyy, and M. Sawicki, *Phys. Rev. B* **84**, 024409 (2011).
  - [24] C. A. M. Mulder, A. J. van Duynveldt, and J. A. Mydosh, *Phys. Rev. B* **25**, 515 (1982).
  - [25] S. Süllow, G. J. Nieuwenhuys, A. A. Menovsky, J. A. Mydosh, S. A. M. Mentink, T. E. Mason, and W. J. L. Buyers, *Phys. Rev. Lett.* **78**, 354 (1997).
  - [26] R. Mahendiran, Y. Bréard, M. Hervieu, B. Raveau, and P. Schiffer, *Phys. Rev. B* **68**, 104402 (2003).
  - [27] J. A. Mydosh, *Reports on Progress in Physics* **78**, 052501 (2015).
  - [28] J. A. Mydosh, *Spin Glasses: An Experimental Introduction* (Taylor & Francis, London, 1993).
  - [29] S. Chatterjee, S. Giri, S. K. De, and S. Majumdar, *Phys. Rev. B* **79**, 092410 (2009).
  - [30] Q. Luo, D. Q. Zhao, M. X. Pan, and W. H. Wang, *Appl. Phys. Lett.* **92**, 011923 (2008).
  - [31] M. Viswanathan and P. S. A. Kumar, *Phys. Rev. B* **80**, 012410 (2009).
  - [32] D. S. Fisher and D. A. Huse, *Phys. Rev. Lett.* **56**, 1601 (1986).
  - [33] J. Dho, W. S. Kim, and N. H. Hur, *Phys. Rev. Lett.* **89**, 027202 (2002).
  - [34] N. Hanasaki, K. Watanabe, T. Ohtsuka, I. Kézsmárki, S. Iguchi, S. Miyasaka, and Y. Tokura, *Phys. Rev. Lett.* **99**, 086401 (2007).
  - [35] D. N. H. Nam, R. Mathieu, P. Nordblad, N. V. Khiem,

- and N. X. Phuc, *Phys. Rev. B* **62**, 8989 (2000).
- [36] A. Bhattacharyya, S. Giri, and S. Majumdar, *Phys. Rev. B* **83**, 134427 (2011).
- [37] B. Maji, K. G. Suresh, and A. K. Nigam, *Journal of Physics: Condensed Matter* **23**, 506002 (2011).
- [38] M. Sasaki, P. E. Jönsson, H. Takayama, and H. Mamiya, *Phys. Rev. B* **71**, 104405 (2005).
- [39] D. S. Fisher and D. A. Huse, *Phys. Rev. B* **38**, 373 (1988).
- [40] D. S. Fisher and D. A. Huse, *Phys. Rev. B* **38**, 386 (1988).
- [41] S. Kundu, T. Dey, M. Prinz-Zwick, N. Büttgen, and A. V. Mahajan, *Journal of Magnetism and Magnetic Materials* **481**, 77 (2019).
- [42] E. S. R. Gopal, *Specific Heats at Low Temperatures* (Plenum Press, New York, 1966).
- [43] R. Kumar, D. Sheptyakov, P. Khuntia, K. Rolfs, P. G. Freeman, H. M. Rønnow, T. Dey, M. Baenitz, and A. V. Mahajan, *Phys. Rev. B* **94**, 174410 (2016).
- [44] Brando, M., Büttgen, N., Fritsch, V., Hemberger, J., Kaps, H., Krug von Nidda, H.-A., Nicklas, M., Pucher, K., Trinkl, W., Loidl, A., Scheidt, E. W., Klemm, M., and Horn, S., *Eur. Phys. J. B* **25**, 289 (2002).
- [45] W. Trinkl, N. Büttgen, H. Kaps, A. Loidl, M. Klemm, and S. Horn, *Phys. Rev. B* **62**, 1793 (2000).
- [46] M. Schmidt, F. M. Zimmer, and S. G. Magalhaes, *Journal of Physics: Condensed Matter* **29**, 165801 (2017).
- [47] G. Chen, H.-Y. Kee, and Y. B. Kim, *Phys. Rev. Lett.* **113**, 197202 (2014).
- [48] G. Chen, H.-Y. Kee, and Y. B. Kim, *Phys. Rev. B* **93**, 245134 (2016).
- [49] G. Chen and P. A. Lee, *Phys. Rev. B* **97**, 035124 (2018).
- [50] E. C. Andrade, J. A. Hoyos, S. Rachel, and M. Vojta, *Phys. Rev. Lett.* **120**, 097204 (2018).